Finite element simulation of resistance spot welding of advanced high strength steels

A Project Report

submitted by

K VENKATESH

in partial fulfilment of the requirements
for the award of the degree of

MASTER OF TECHNOLOGY

DEPARTMENT OF METALLURGICAL & MATERIALS ENGINEERING
INDIAN INSTITUTE OF TECHNOLOGY MADRAS.

May 2018

THESIS CERTIFICATE

This is to certify that the thesis titled Finite element simulation of resistance spot welding of advanced high strength steels, submitted by **K Venkatesh**, to the Indian Institute of Technology, Madras, for the award of the degree of **Master of Technology**, is a bona fide record of the research work done by him under my supervision. The contents of this thesis, in full or in parts, have not been submitted to any other Institute or University for the award of any degree or diploma.

Dr. Murugaiyan Amirthalingam
Research Guide
Assistant Professor
Dept. of Metallurgical & Materials Engineering
IIT-Madras, 600 036

Place: Chennai

Date: 16th May 2018

ACKNOWLEDGEMENTS

I am deeply grateful to my guide, Dr. Murugaiyan Amirthalingam for his persistent guidance and support, without which this thesis would not have fructified. I wish to thank the students and staff at Materials Joining Laboratory, particularly Mr. Rangan K for helping me perform experiments on Gleeble as well as operating the resistance spot welding machine; and Mr. M Ramakishore & Mr. Melvin for helping me get my samples cut using Electric Discharge Machining (EDM). I also wish to thank Mr. Deepu Mathew for providing materials property data from JMatPro; Mr. Anirban for operating the surface profilometer; and Mr. Joe Jacob for tips on modifying the solver settings. I also wish to thank my friends and family for supporting me throughout the length of my stay at IIT Madras.

ABSTRACT

KEYWORDS: Resistance spot welding, interface resistance, finite element method, advanced high strength steels

In recent years, great emphasis is being laid on reducing the weight of automobiles in order to reduce their CO_2 emissions. In order to accomplish the goal, efforts are made to develop 3rd generation Advanced High Strength Steels (AHSS) with strength levels of 1 GPa or higher, mainly by increasing alloying content in these steels. Small amounts of phosphorus is also added for (i) solid solution strengthening and (ii) stabilizing retained austenite in the microstructures. However, when these steels are resistance spot welded, the segregation of alloying elements occurs during solidification, resulting in cracking during welding and brittle weld metal failure upon loading. Weld metal strength was found to be particularly sensitive to phosphorus segregation. Since resistance spot welding is the most widely used joining process to fabricate automotive parts, it is imperative to modify the weld thermal-mechanical cycles suitably to reduce elemental segregation. The application of a dual current pulse was found to reduce segregation and improve mechanical properties.

Recent attempts to simulate elemental segregation during weld metal solidification using phase field modeling have succeeded in qualitatively capturing the elemental segregation trends; however, a quantitative match with experiments remains elusive, as arbitrary temperature-time profiles at the weld pool were used to run the simulations. In order to obtain quantitatively accurate phase field simulations, it is imperative to use the actual temperature profiles experienced in the weld nugget for performing phase field simulations, which can be obtained from finite element simulation of resistance spot welding. In this study, we investigate the effect of various process and model parameters on the accuracy and computational cost of performing finite element simulations of resistance spot welding.

TABLE OF CONTENTS

LIST OF TABLES

LIST OF FIGURES

ABBREVIATIONS

EDM	Electric Discharge Machining
AHSS	Advanced High Strength Steels
DP	Dual Phase
TRIP	TRansformation Induced Plasticity
HF	Hot Forming
RSW	Resistance Spot Welding
JMatPro	Java based Materails Properties

NOTATION

$Q_j(t)$	Joule heat
$I(t)$	Current
$R(t)$	Resistance
t	time
$R1$	Top electrode-top sheet electrical resistance
$R2$	Top sheet bulk electrical resistance
$R3$	Sheet-sheet electrical interface resistance
$R4$	Bottom sheet bulk electrical resistance
$R5$	Bottom sheet-bottom electrode electrical resistance
T_0	Room temperature
l_0	Sheet-sheet gap at room temperature
a_0	Real area of contact at room temperature
l	Sheet-sheet gap at any temperature T
a	Real area of contact at any temperature T
$\sigma(T)$	Yield strength at any temperature T
$\rho(T)$	Density at any temperature T
$R(T)$	Sheet-sheet electrical contact resistance at any temperature T
P	Load applied by electrodes
$\rho_e(T)$	Electrical resistivity of sheet material at any temperature T

CHAPTER 1

INTRODUCTION

1.1 Motivation

Rapid increase in the number of automobiles plying in the roads of many major cities has resulted in a serious deterioration of air quality over the years due to the release of noxious emissions from automobiles [1,2]. Consequently, governments across the globe have imposed stringent vehicle exhaust norms in a bid to mitigate air pollution [3,4]. Great emphasis is being placed on reducing the weight of the automobile, as a lighter car would require less energy for propulsion, and hence a concomitant reduction in the emissions generated per km travelled is expected. This is to be accomplished without any compromise in the structural integrity of the automobile, which would only be made possible by using high strength materials to manufacture the components of the vehicle [10]. Therefore, the automotive industry is increasingly resorting to the use of Advanced High Strength Steels (AHSS) such as Dual Phase (DP) steels, TRIP (Transformation Induced Plasticity) steels and HF (Hot Forming) steels to fabricate the various components of a vehicle [5,6]. These steels possess high strength with reasonable ductility, made possible by carefully tailoring the alloy chemistry and heat treatment procedure [7].

In order to fabricate the automotive chassis, these components need to be welded together, with resistance spot welding being the most popular due to the attractive combination of low cost, high degree of automation, high efficiency and high productivity [8]. A modern automobile contains about 4000 spot welds [12]. However, the microstructure gets altered during the process of welding due to the imposition of thermal cycles, resulting in a hard, martensitic microstructure with high level of segregation of alloying elements, prone to brittle failure with low strength levels [7]. Therefore, recent efforts are directed towards modifying welding processes so as to yield spot welds with improved mechanical properties. [7-9].

Phosphorus, which is added to these steels for the purpose of solid solution strengthening and stabilizing retained austenite, tends to segregate to the grain boundaries during solidification, resulting in brittle grain boundaries [7,11]. Additionally, the grain orientation in the fusion zone is perpendicular to the loading direction in the case of peel loading, thereby providing an easy pathway for crack propagation. Steels containing phosphorus was found to fail at a lower load when compared to steels without phosphorus but otherwise having the same composition [9]. Post pulsing, or the application of a current pulse subsequent to the primary pulse, was found to reduce phosphorus segregation, and a marked improvement in weld strength and ductility was observed without any significant changes in the nugget geometry or hardness [8,9]. Determination of optimum process parameters through experiments is laborious and time consuming. Therefore, it is imperative to develop computational tools to simulate resistance spot welding and the weld microstructure [12].

The combination of finite element and phase field modelling has been successfully used to obtain the thermal profile and microstructure of resistance spot welds having good qualitative agreement with experimental results; however, a quantitative match between simulation and experimental results was not achieved, as a simple, linear temperature profile with low heating and cooling rates was used [9]. In order to accomplish the goal of using the thermal profile obtained from the finite element model as an input for the phase field model, it is imperative to accurately model resistance spot welding. In this study, we develop a model of resistance spot welding and perform simulations using COMSOL Multiphysics, a commercial finite element software. We study the effect of various process parameters on the thermal profile in the sheet.

1.2 Resistance spot welding

In resistance spot welding (RSW), metal sheets are joined together by electrical resistance instead of an electric arc, which is the case in arc welding. RSW joins small pieces of the materials (spots) together by applying a current through them while they are pressed together by a pair of water cooled copper electrodes. Due to the applied current, localized melting occurs due to resistance heating, which joins the sheets together at the spot where the current is applied. The application of force by the electrodes help keep the sheets aligned perfectly. The electrode force is maintained even after the current is cut off, to prevent lateral movement and to ensure fast solidification.

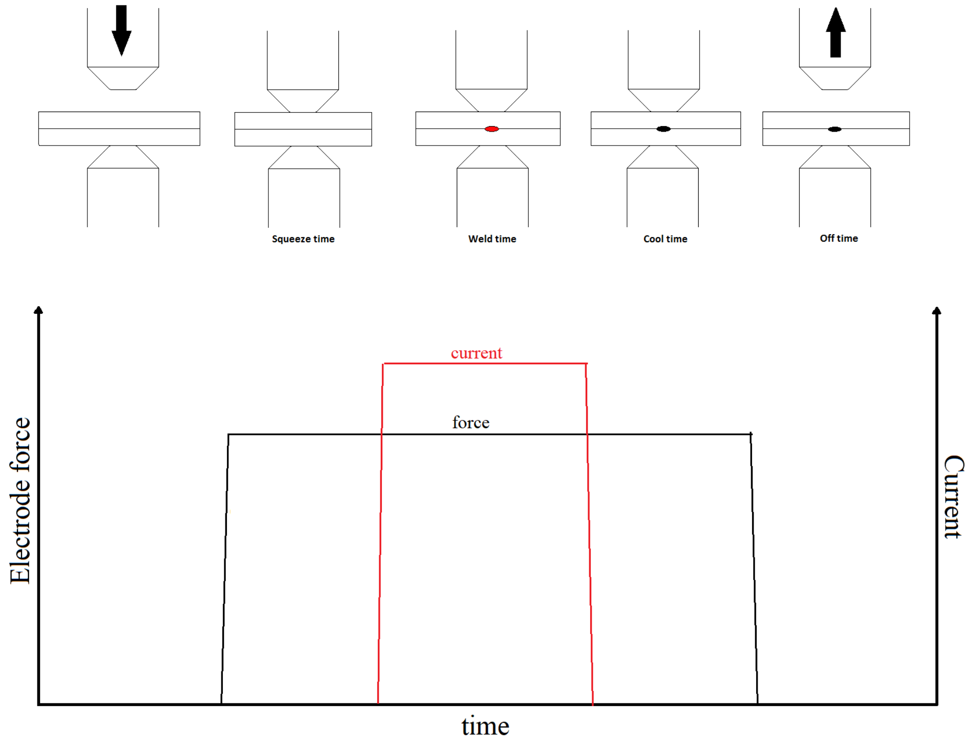

Figure 1.1: Resistance spot welding timeline

The heat generated due to resistance heating is given by Joule's law:

$$Q_J(t) = \int I^2(t)R(t)dt$$

$Q_J(t)$ is the heat energy generated, I(t) is the current, R(t) is the resistance and t is the time [13]. Due to the heat generated, the temperature in the sheet rises and exceeds the melting point of the metal (provided the current is sufficiently high), resulting in the formation of molten metal. Once the current is cut off, the molten pool solidifies due to heat dissipation, primarily through conduction [14]. The resistances encountered in a two sheet stack is shown in figure 1.2. R1 and R5 are the electrode-sheet electrical resistances, R2 and R4 are the bulk electrical resistance of the sheets and R3 is the sheet-sheet electrical resistance.

The contact resistance between the sheets is substantially higher during the initial stages of welding. This resistance arises due to (i) constriction in the current flow, and (ii) resistance due to film/contaminants on the surface. Due to low strength and high

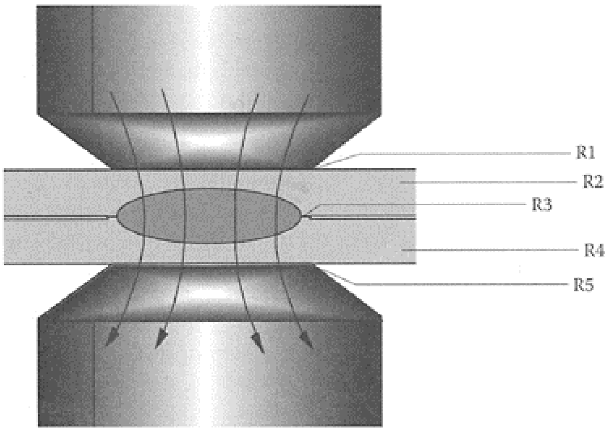

Figure 1.2: Resistances in resistance spot welding [12]

electrical conductivity of copper, the electrical resistance at the electrode-sheet interface can be neglected. The contact resistance in an interface is dependent of the contact area, and evolves with time as a result of deformation. The increase in contact area, caused by the increase in temperature (which reduces the yield strength of the material) decreases the current density, which in turn decreases the electrical resistance at the interface.

1.3 Parameters in resistance spot welding process

In resistance spot welding, the important process parameters are welding current, electrode force, weld time and cool time.

1.3.1 Welding current

The weld current is the dominant parameter in this welding process since the generated heat is proportional to the square of the current. If the current is too high it may cause expulsion, which in turn decreases the nugget size and causes splashes of molten material at other parts of the construction, which then have to be removed and causes time-consuming repair work. Using a current that is too high can also lead to large deformations and indentations on the sheets, as well as more wear on the electrodes. On the other hand, a current that is too low will have a very low heat input, resulting in a very small weld nugget, which will have poor load bearing capability. Therefore, it is important to use the correct welding current in order to ensure a good weld. Typically, a weld current of about 5kA is used for steel sheets [9][13].

1.3.2 Electrode force

The electrode force is applied to ensure that the alignment of the sheets is not disturbed during welding. Too low an electrode force may cause the alignment to change. If the electrode force is too high, the electrodes will penetrate very deeply into the sheet, resulting in poor weld surface appearance and high indentation depth. Typically, an electrode force in the range of 4kN is applied for steel sheets [14][15].

1.3.3 Weld time

The weld time is the time duration for which the current is passed through the electrodes. If the weld time is too high, expulsion of molten metal will occur, resulting in poor properties and aesthetics. If the weld time is too low, then adequate heating may not occur, resulting in small weld nuggets or even the absence of a weld nugget. From the point of view of reducing costs, it is desirable to reduce the weld time in order to improve productivity, which can be compensated by increasing the welding current. Typically, the weld time will be of the order of 200 milliseconds [9][14].

1.3.4 Cool time

The cool time refers to the time gap between current cut-off and electrode removal. The electrodes must continue to clamp the joint together even after the current has been cut off, to ensure that the stresses during cooling do not cause any misalignment. However, if the cool time is too high, the productivity will be affected.

1.3.5 Electrode material

The electrodes play two important roles in resistance spot welding: (i) to clamp the sheets together, and (ii) to apply high current through the sheets. In order to reduce heating of the electrodes, copper and copper alloys are typically used to fabricate the electrodes. These electrodes are water cooled to ensure that the electrodes do not get heated up, which will soften due to heating and hence cause the electrode shape to change. The electrode materials are described in ISO 5182:2008 standard [16].

1.3.6 Electrode geometry

The geometry of the electrode determines the nature of the contact between the electrode and the sheets, which in turn affects both the contact pressure and the current distribution. A number of common electrode geometries is shown in the figure below. The geometry of the electrodes are governed by the ISO 5821:2009 standard [17].

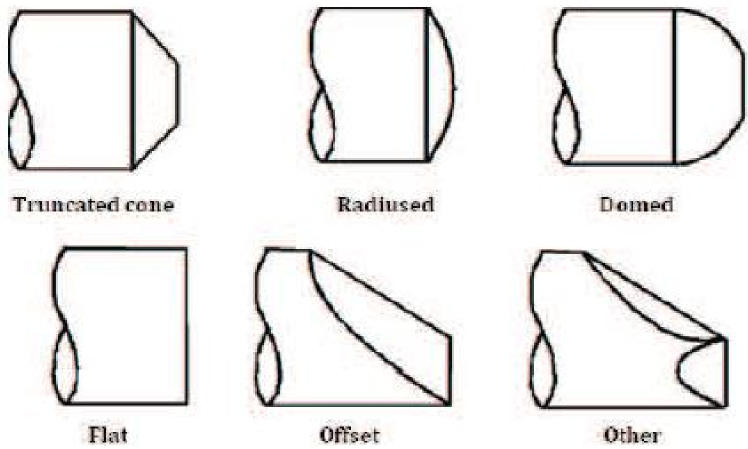

Figure 1.3: Common electrode geometries [13]

CHAPTER 2

Literature review

2.1 Resistance spot welding simulation

Greenwood in 1961 [18] developed the first heat conduction model to simulate the temperature profile evolution during resistance spot welding. Another finite difference based one dimensional heat transfer model was reported by Gould, J. E. [19]. Both these models fail to predict nugget formation as they, being one dimensional models, do not consider radial heat transfer. Later, two dimensional axisymmetric heat transfer models for analyzing this welding process were reported by Cho et al. [20], Han et al. [21], Wei et al. [22, 23] where they used finite difference method. Unfortunately, these models focused attention on heat transfer only, while neglecting the thermal-electrical nature of the process. Also, variation of contact resistance was considered in an arbitrary manner. Nishiguchi et al. [24] reported an improved version of such an axisymmetric model. Apart from heat transfer analysis, this model considered electrical field analysis and elasto-plastic analysis. However, the influence of contact resistance was neglected. Finite element method has been successfully used to simulate resistance spot welding [25-32]. Both electro-thermal as well as electro-thermo-mechanical coupling have been incorporated in these models. The sheet-sheet contact resistance, which varies with temperature, was found to have a profound influence on the weld nugget diameter. Therefore, accurate simulation of resistance spot welding requires accurate contact resistance data as a function of temperature.

2.2 Electrical contact resistance

Electrical contact resistance arises due to constriction to the flow of current at the interface due to the presence of asperities at the surface of the bodies in contact, and due to presence of surface film of oxides or other contaminants. The contact resistance is affected by both pressure and temperature. Increase in pressure increases the area of contact, thereby reducing the local current densities at the asperities and reducing the resistance. Increase in temperature also affects the contact resistance due to changes in electrical resistance, yield strength and thermal expansion. The contact resistance is also dependent on materials properties. As contact resistances show high dependency on temperature, pressure and contact configuration, large range of contact resistance values, varying in several orders of magnitude, are encountered [33].

2.2.1 Experiments

Feulvarch et al. [34] experimentally measured the interface resistance of unalloyed, uncoated steel sheets to be in the range of $3 \times 10^{-11}\,\Omega m^2$ to $10^{-8}\,\Omega m^2$. Robin et al. [35] experimentally measured the interface resistance to be in the range of $4 \times 10^{-10}\,\Omega m^2$ to $5 \times 10^{-9}\,\Omega m^2$. Babu et al. [36] determined the electrical contact resistance of uncoated, plain carbon steel sheets to be $10^{-7}\,\Omega m^2$ at 20 MPa and $4 \times 10^{-6}\,\Omega m^2$ at 80 MPa pressure at room temperature. The interface resistance was found to vary inversely with pressure. Song et al. [37] measured the interface resistance of AISI 1018 low carbon steel to be $4.5 \times 10^{-8}\,\Omega m^2$ at room temperature at 100 MPa pressure. Bao et al. [38] studied the effect of temperature and pressure on electrical contact resistance of electro-galvanized chromium-free, electro-galvanized fingerprint-resistant, electro-galvanized phosphating and hot-dip galvanized chromium-free coated steel sheets. The electrical contact resistance at 110 MPa pressure and room temperature for the hot-dip galvanized sheet was measured to be $3 \times 10^{-7}\,\Omega m^2$.

2.2.2 Modeling

Greenwood [41] developed a model to predict the electrical contact resistance, which requires knowledge of the number of contacting asperities, average radius of contacting asperities and average centre to centre distance of asperities as model input parameters. Cooper et al. [42] developed a statistical contact model for rough surfaces. The model, originally developed to obtain thermal contact resistance, was used to model electrical contact resistance due to the close analogy between thermal and electrical effects. Though the models are quite accurate, it is difficult to calculate temperature-dependent contact resistance due to difficulties in estimating the model input parameters at high temperatures. Hence, there is a need to develop a versatile model to obtain temperature-dependent electrical contact resistance across a wide range of temperatures, relying primarily on the temperature-dependent materials properties as input parameters to effect temperature-dependent variations.

CHAPTER 3

Methodology

COMSOL Multiphysics, a commercial software that enables solving coupled partial differential equations using finite element method was used to model resistance spot welding. Coupling between electrical and thermal physics was considered. Mechanical deformations were not accounted for in this model. The application of electric current results in a non-uniform potential field, the gradient of which gives rise to local currents that cause resistive heating. The resistive heating gives rise to a temperature field, which gives rise to changes in electrical resistivity, as electrical resistivity is a function of temperature. Due to this change in electrical resistivity, the potential field changes. Thus, the electric potential field affects the temperature field and vice-versa. Hence, a coupling between the electrical and thermal physics is necessary in order to accurately simulate resistance spot welding. The schematic of electro-thermal coupling in COMSOL Multiphysics is shown in the figure below.

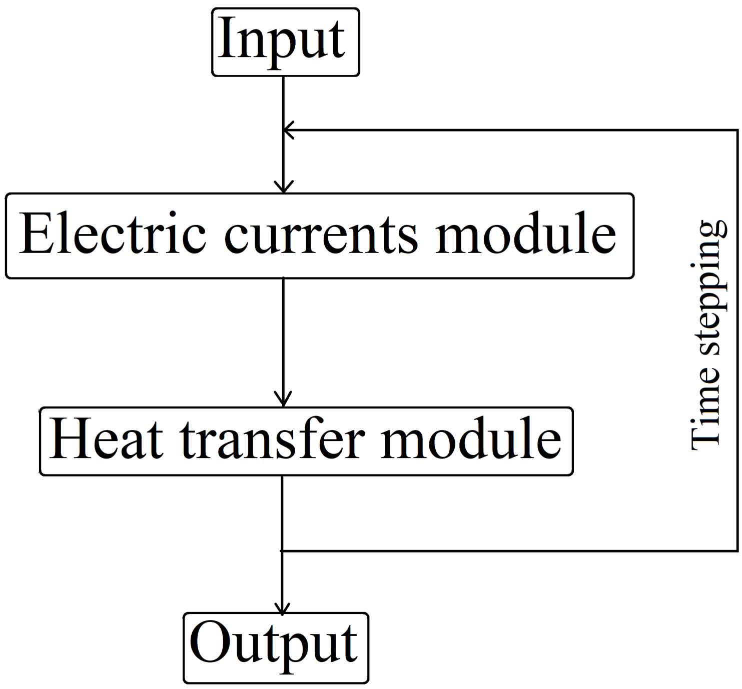

Figure 3.1: Schematic of electro-thermal coupling

3.1 Geometry

The dimensions of the model used for simulation is shown in the figure below. Two sheets of 1.2 mm thickness were used. The dimensions of the electrodes were measured using a vernier caliper. Simulations were run on both 2D axisymmetric model and 3D model. The 3D model was generated by rotating the constructed 2D model around the axis of symmetry.

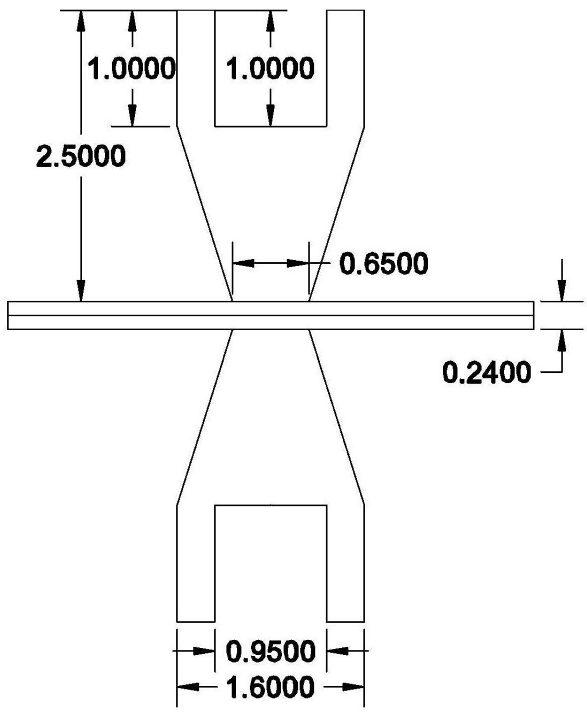

Figure 3.2: Model dimensions

In order to accurately reproduce the features of resistance spot welding of the sheets in a simple electro-thermal model, the interface resistance is to be applied only to that part of the faying surfaces that are in electrical contact. At the faying surface, only a small area of the two sheets are in electrical contact, where the interface resistance derived above is applicable. The remaining area, though in close proximity, is not in electrical contact. Hence, for the parametric model, at a microscopic level, the two sheets are separated by a small distance (0.01 mm) except for the regions that are in contact. The regions in contact are assumed to be coaxial and equal in area to that of the electrode faces.

3.2 Materials properties

The sheets are made of DP1000 alloy. The alloy composition is given in table below. Materials properties were obtained using the software JMatPro.

Table 3.1: DP1000 alloy composition

Element	Composition
C	0.22
Mn	2.9
Si	1.9
P	0.011
Al	0.15
Cr + Mo	1.4
Fe	balance

3.3 Process parameters

The welding process parameters used for the simulations are given in the table below.

Table 3.2: Process parameters

Process parameter	Value
Current	4-8 kA
Electrode force	3.5 kN
Squeeze time	500 ms
Weld time	120 ms
Hold time	380 ms

3.4 Physics settings

3.4.1 Heat transfer settings

- The initial temperature is set to 298K.
- The temperature in the interior surface of the copper electrodes is set to 298K throughout the process.
- The rest of the surfaces are set to be insulating i.e. no heat transfer occurs through the other surfaces open to the atmosphere.

3.4.2 Electrical currents settings

- The voltage at the bottom face of the electrode is set to 0.
- Current is applied from the top face of the electrode.
- Initial voltage is set to 0 throughout the material.
- Contact resistance at the sheet-sheet interface is applied through the 'surface impedance' option.

3.5 Interface resistance model

All unpolished surfaces, which may seem to be perfectly flat to the naked eye, are replete with asperities. As a result, when 2 surfaces come in contact at a macroscopic scale, only the highest points of the asperities come in contact at the microscopic scale, as shown in figure below. In this model, the asperities at the interface are modelled as a set of cylinders as shown in figure.

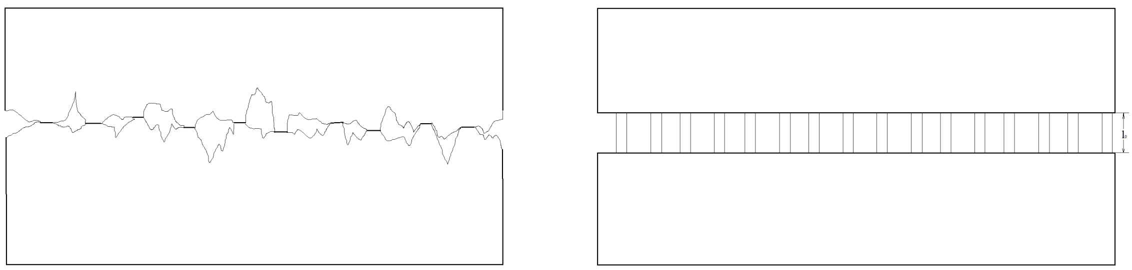

Figure 3.3: Left: Asperities in an unpolished interface; right: model of interface

In this model, the asperities at the interface are modelled as a set of cylinders as shown in figure 4. Let the height and total area of all cylinders at temperature T_0 (room temperature) be l_0 and a_0 respectively, and the height and total area of all the cylinders at a temperature T be l and a respectively. Let $\sigma(T)$ be the yield strength at temperature T, $\rho(T)$ be the density at temperature T, R(T) be the interface resistance at temperature T and P be the load applied by the electrodes. We know that

$$\frac{P}{a} = \sigma(T) \quad i.e. \quad a = \frac{P}{\sigma(T)} \tag{3.1}$$

From the conservation of mass, we have

$$\rho(T_0) \times v_0 = \rho(T) \times v$$

i.e.

$$\rho(T_0) \times l_0 \times a_0 = \rho(T) \times l \times a$$

Substituting eq. (3.1) here, we get

$$\frac{\rho(T_0) \times P \times l_0}{\sigma(T_0)} = \frac{\rho(T) \times P \times l}{\sigma(T)}$$

i.e.

$$\frac{\rho(T_0) \times l_0}{\sigma(T_0)} = \frac{\rho(T) \times l}{\sigma(T)}$$

Rearranging, we get

$$l = l_0 \times \frac{\rho(T_0)}{\rho(T)} \times \frac{\sigma(T)}{\sigma(T_0)} \tag{3.2}$$

We know that

$$R = \frac{\rho_e \times l}{a}$$

Substituting eq. (3.2) and eq. (3.1) here, we get

$$R = \rho_e(T) \times (\frac{\rho(T_0)}{\rho(T)} \times \frac{\sigma(T)}{\sigma(T_0)} \times l_0) \times (\frac{\sigma(T)}{P})$$

which simplifies to

$$R = \rho_e(T) \times \frac{\sigma^2(T) \times \rho(T_0)}{\sigma(T_0) \times P \times \rho(T)} \times l_0 \tag{3.3}$$

The validity of the above equation can be tested using some of the properties of interface resistance that are known to us a priori. The parameter l_0 can be treated as a quantity that is used to capture the surface roughness that is inherent to all surfaces. It is easy to see that if $l_0 \to 0, R \to 0$ i.e. if the surfaces are perfectly flat, then the interface resistance drops to zero, which is logical, as the very source of interface resistance is the presence of asperities, which result in an imperfect contact at the interface. It can also be derived that the interface resistance R drops to zero when $\sigma(T)$ drops to zero i.e. when liquid forms. Again, this can be corroborated by our intuitive understanding of perfect contact at the interface in presence of a liquid. It can also be shown that the equation is dimensionally consistent. An equivalent derivation for the thermal resistance can be derived; however, we neglect the thermal resistance of the faying surface, as the heat flow across the sheet-sheet interface is zero due to symmetry. We also neglect the electrode-sheet interface resistance.

CHAPTER 4

Results

4.1 Materials properties

Materials properties were obtained from JMatPro software. JMatPro is an acronym for **J**ava based **Mat**erials **Pro**perties. The software is used to calculate thermophysical and physical properties (from room temperature to the liquid state), time-temperature-transformation/continuous-cooling transformation diagrams, stress/strain diagrams, proof and tensile stress, hardness and creep properties. The calculations are based on sound physical principles rather than purely statistical methods, thus overcoming the limitations of methods such as regression analysis [39].

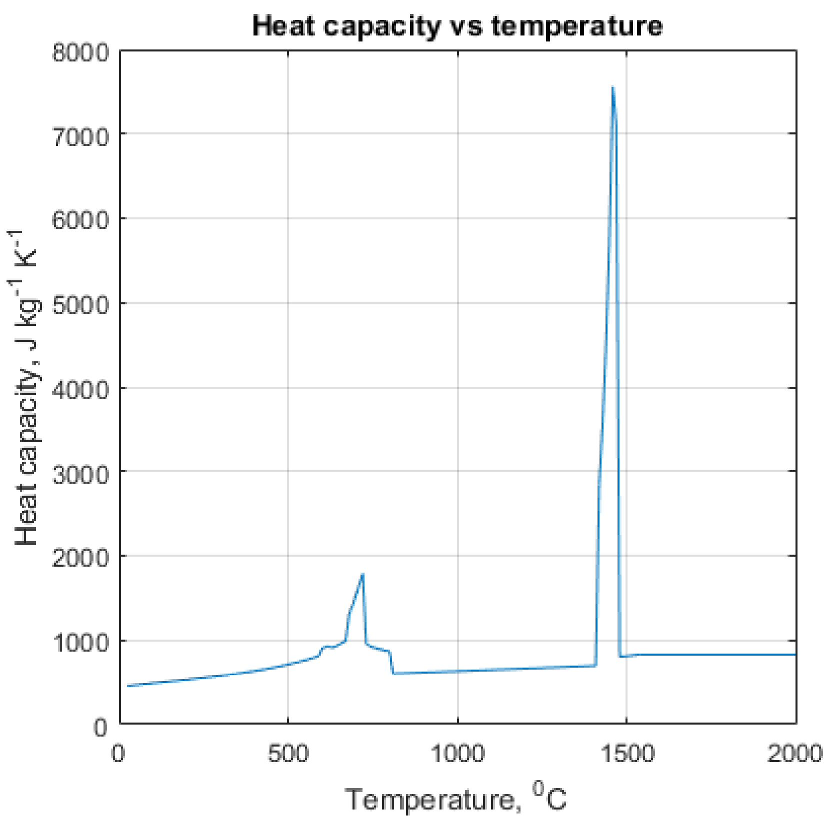

Figure 4.1: Plot of heat capacity vs temperature, DP1000 steel

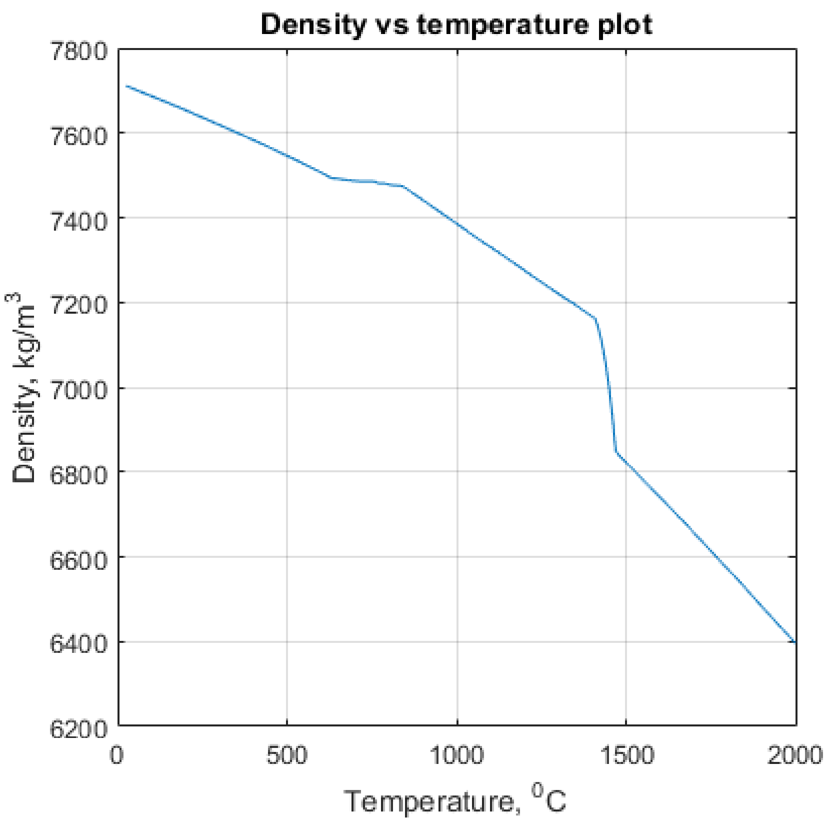

Figure 4.2: Plot of density vs temperature, DP1000 steel

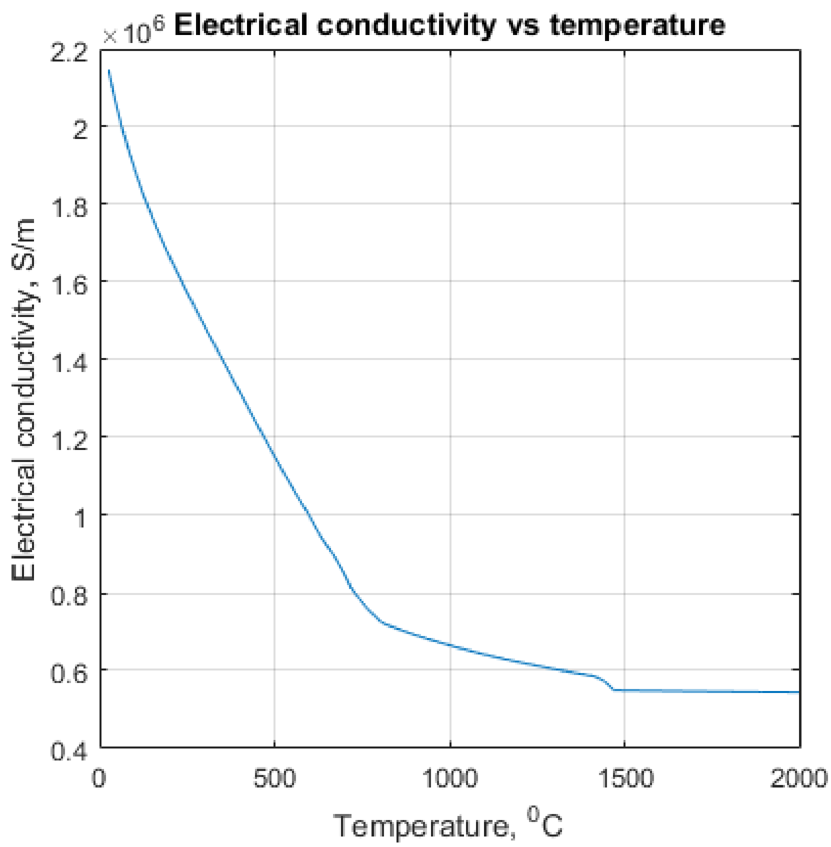

Figure 4.3: Plot of electrical conductivity vs temperature, DP1000 steel

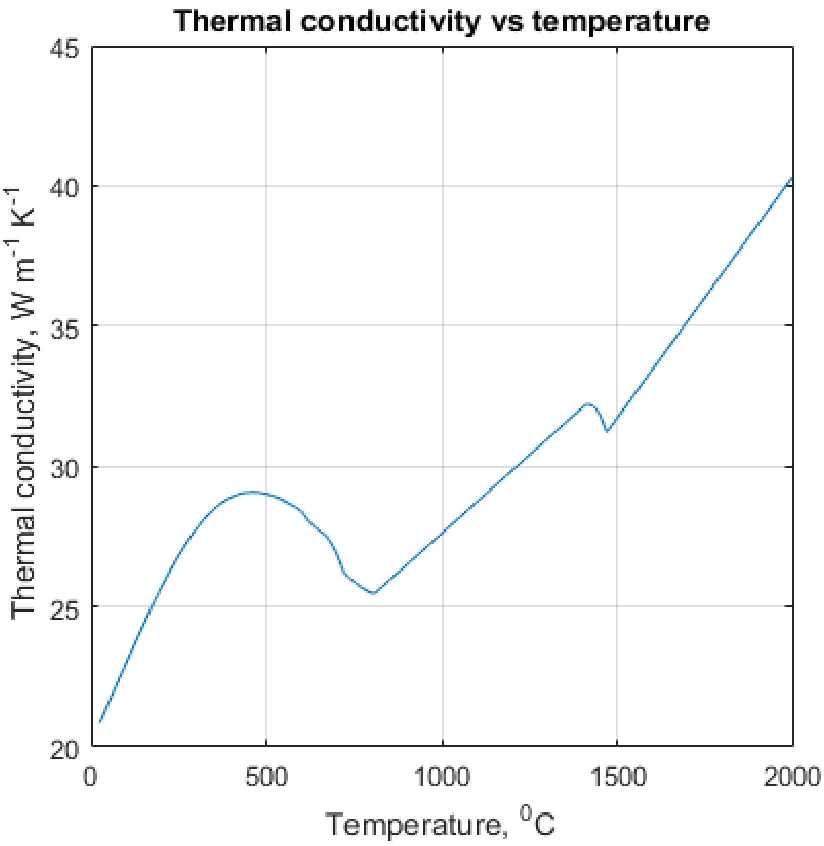

Figure 4.4: Plot of thermal conductivity vs temperature, DP1000 steel

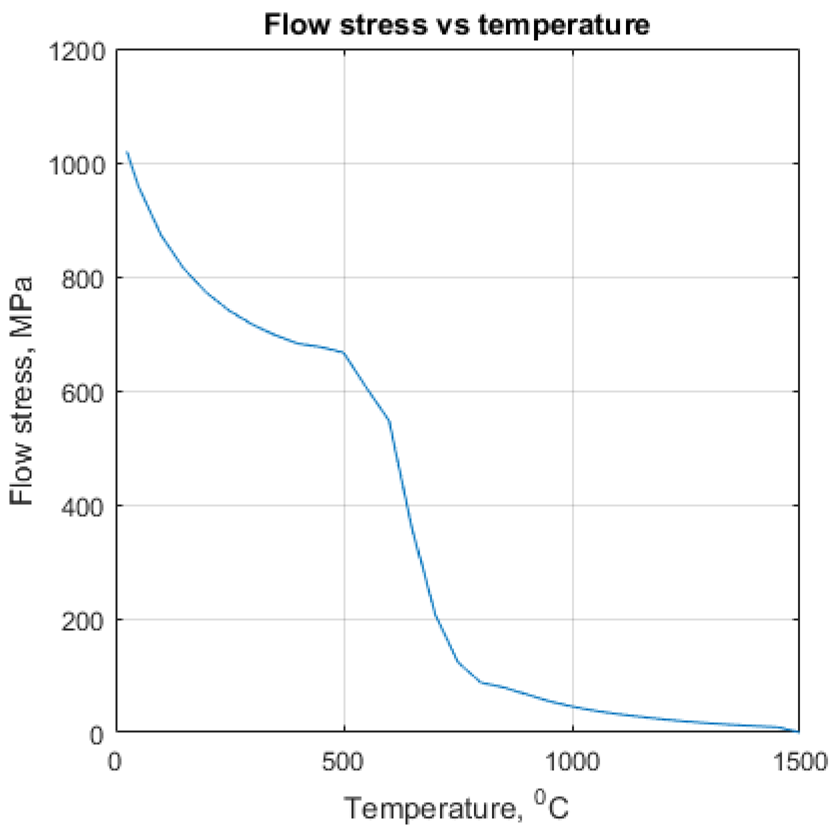

Figure 4.5: Plot of flow stress vs temperature, DP1000 steel

4.2 Interface resistance

The interface resistance vs temperature as predicted by the model is shown in the figure below. The interface resistance function predicted by the model was used as an input for the finite element simulations. A correction factor of 10^4 was used to account for film resistance. The choice of correction factor was based on the experimentally measured sheet-sheet interface resistance value at room temperature for sheets having similar surface conditions and materials properties.

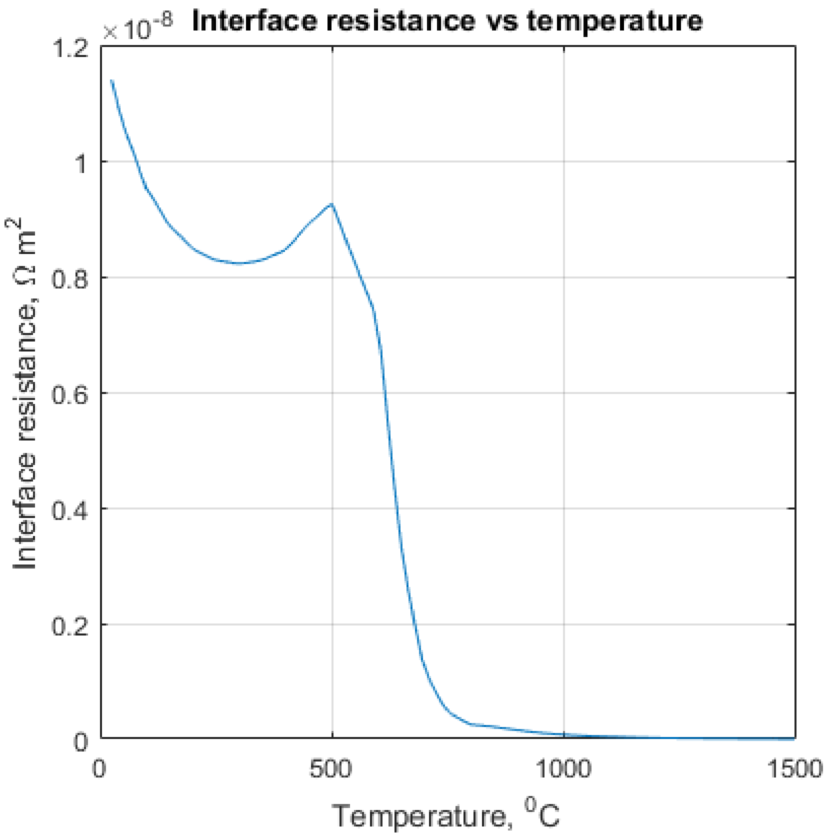

Figure 4.6: Plot of sheet-sheet interface resistance vs temperature, DP1000 steel

4.3 Effect of geometry

Simulations were run using both 2D axisymmetric as well as 3D models. The temperature profile at 220 ms is shown in the figures below. Both the temperature profiles were obtained with 5 kA current and normal mesh size.

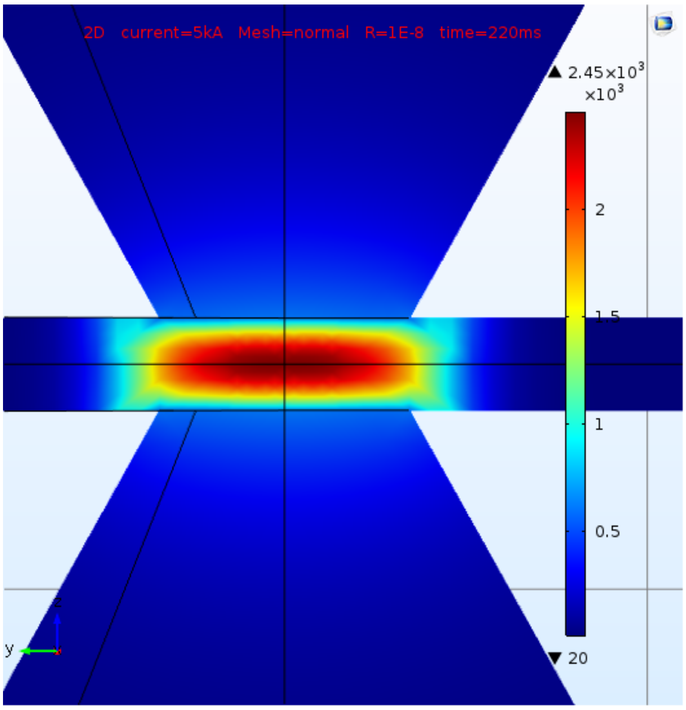

Figure 4.7: Temperature profile, 2D axisymmetric model

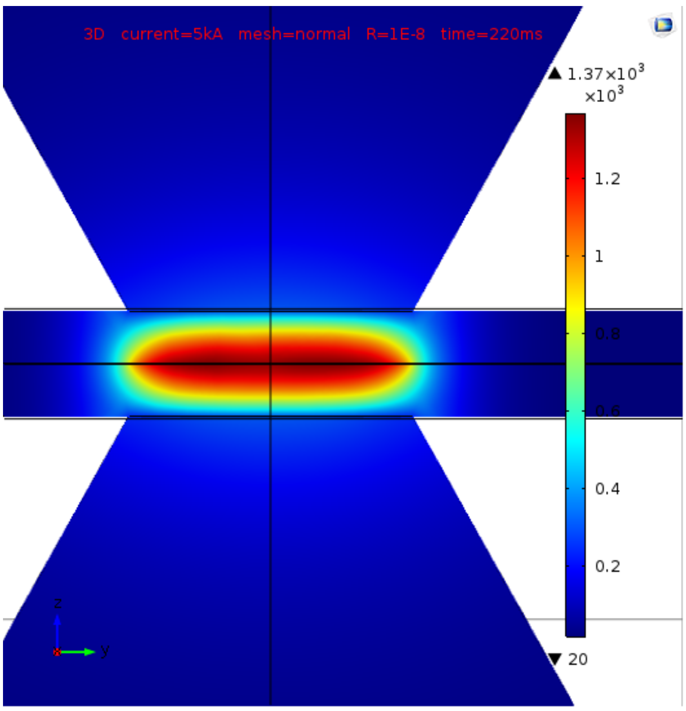

Figure 4.8: Temperature profile, 3D model

4.4 Effect of interface resistance

Simulations were performed on models with and without incorporating the interface resistance. The other process parameters were kept the same in order to draw meaningful information from the simulation results.

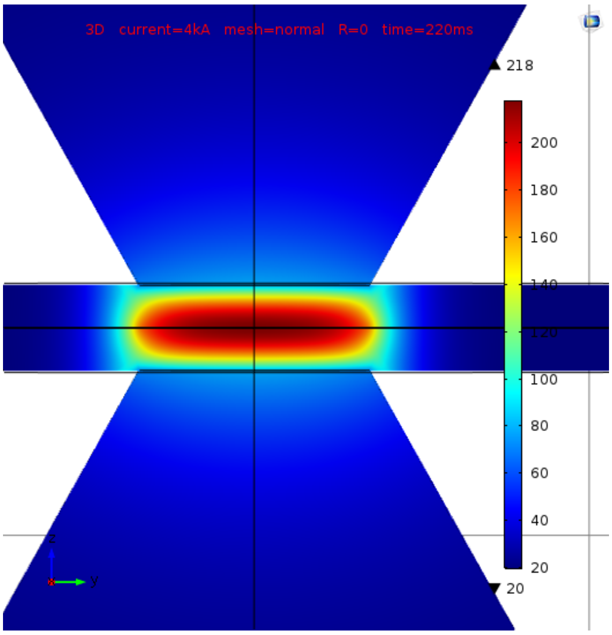

Figure 4.9: Temperature profile, no interface resistance

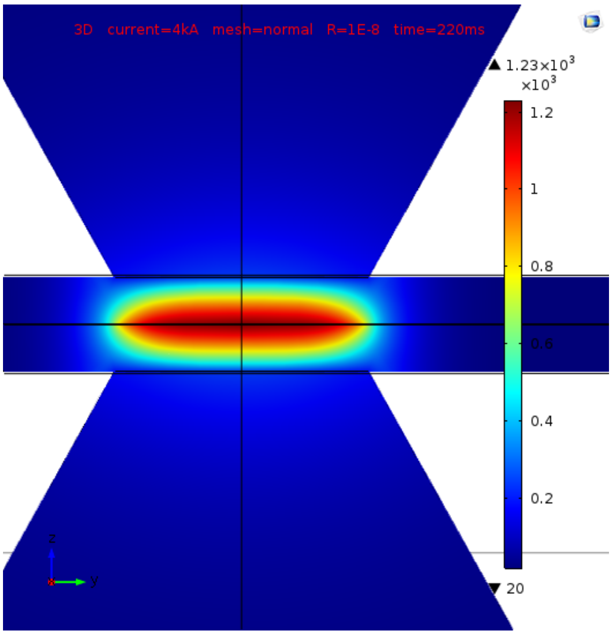

Figure 4.10: Temperature profile, with interface resistance

4.5 Effect of welding current on temperature profile

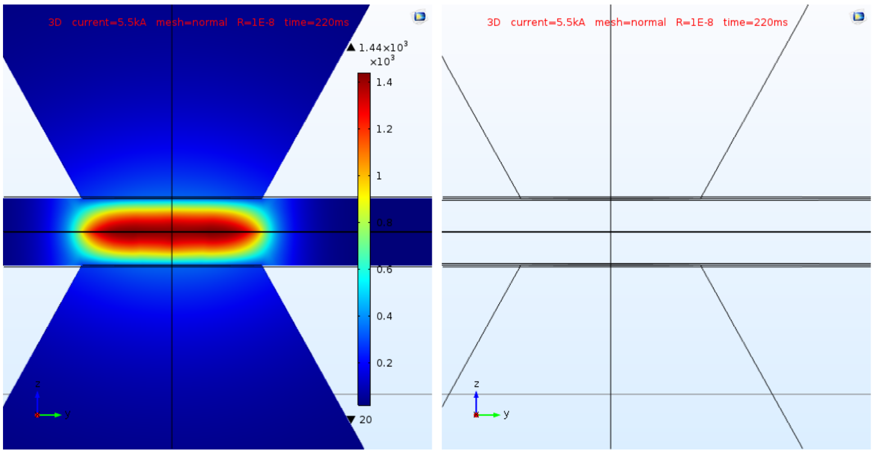

Figure 4.11: Temperature profile and molten pool, 5.5 kA

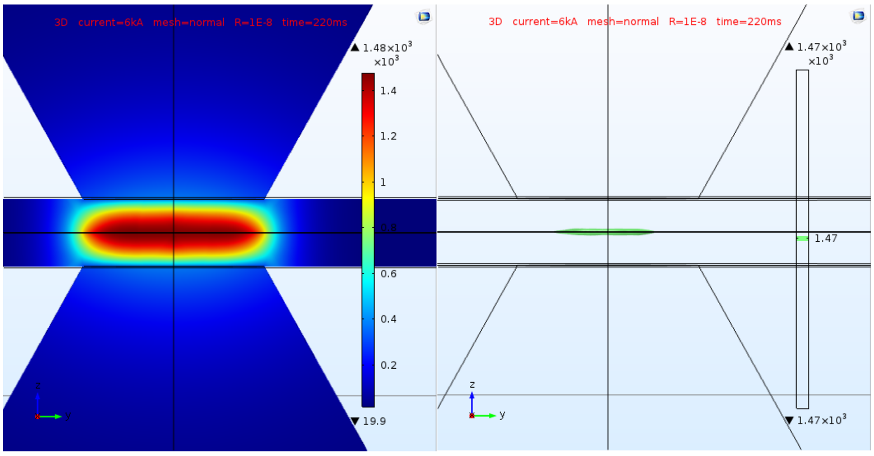

Figure 4.12: Temperature profile and molten pool, 6 kA

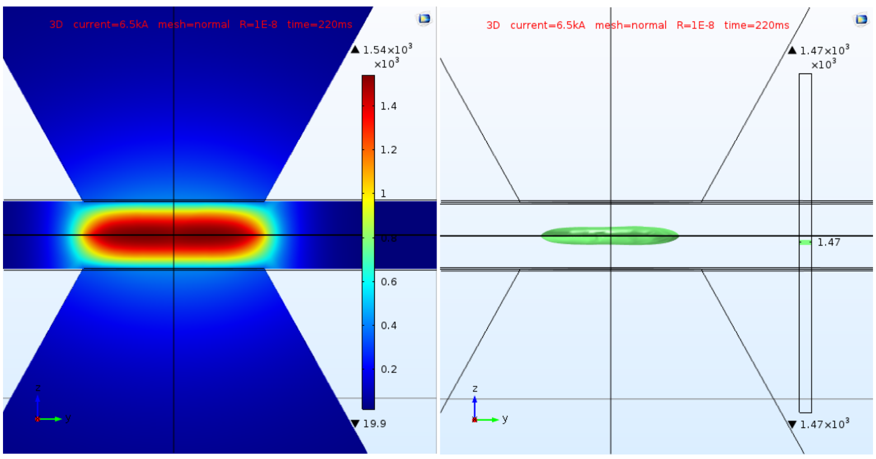

Figure 4.13: Temperature profile and molten pool, 6.5 kA

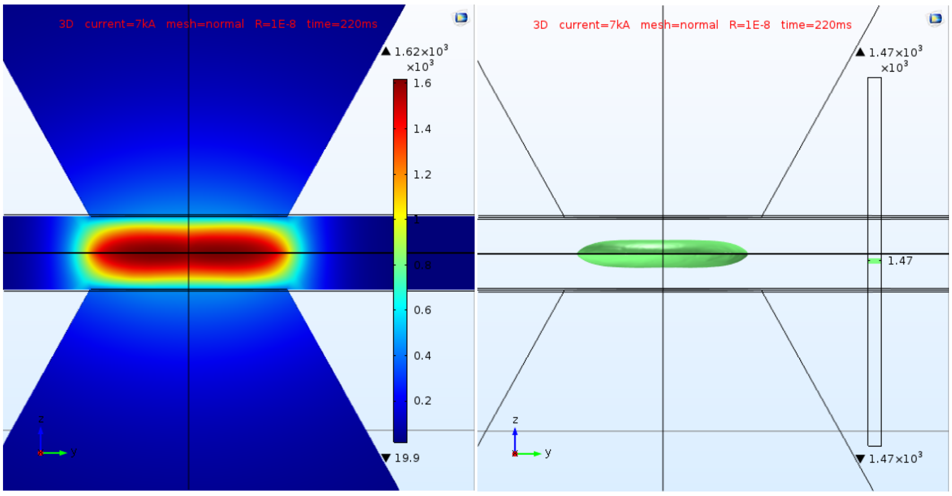

Figure 4.14: Temperature profile and molten pool, 7 kA

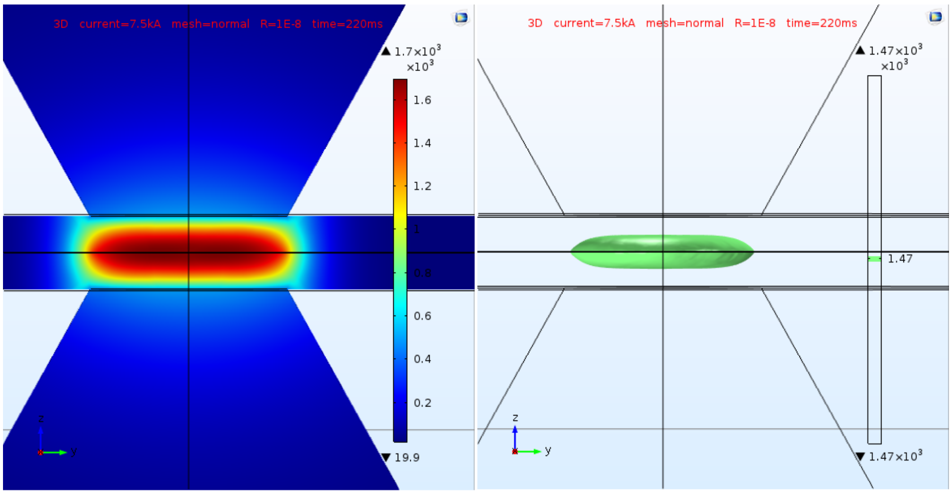

Figure 4.15: Temperature profile and molten pool, 7.5 kA

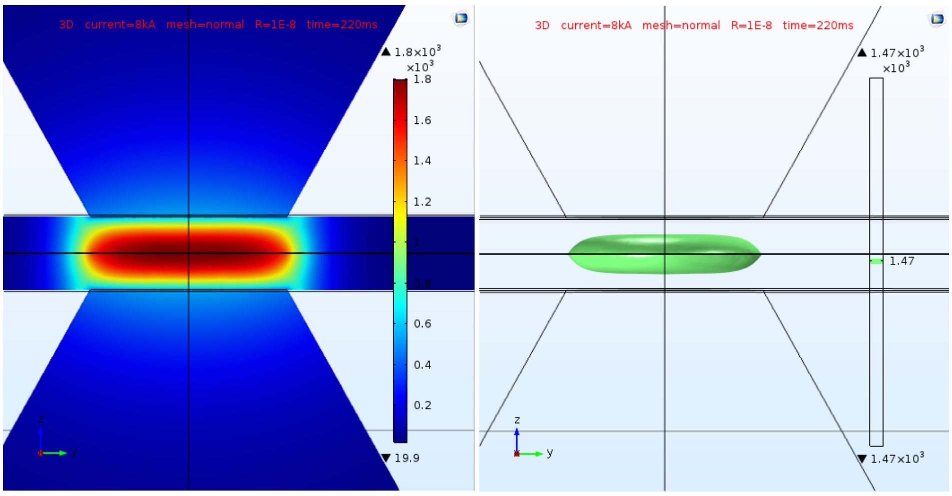

Figure 4.16: Temperature profile and molten pool, 8 kA

4.6 Evolution of temperature profile with time

The temperature profile at certain specific points as a function of time is plotted in the figure below. The center point is the point at the centre of the two sheets. The point marked 0.2 mm is located 0.2 mm below the centre point along the axis of symmetry, the point marked 0.4 mm is located 0.4 mm below the centre point along the axis of symmetry and so on.

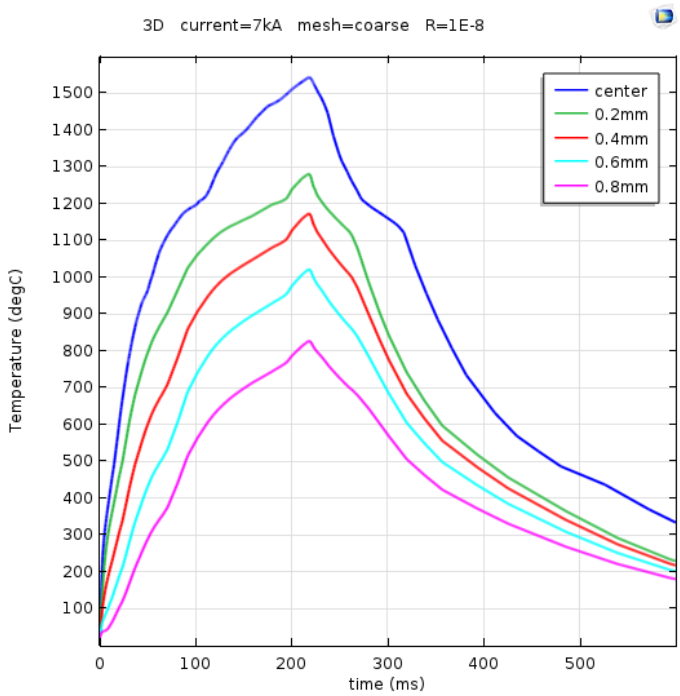

Figure 4.17: Temperature profile, 3D model

CHAPTER 5

Discussion

5.1 Effect of geometry

For the 2D axisymmetric model, certain anomalies are observed in the temperature profile, particularly at the center of the weld pool. Similar anomaly was observed in the temperature contours of De et al. [40]. Also, the peak temperature and size of molten pool is substantially higher when compared to the results from the 3D model. Unlike the 3D model, lack of symmetry between the top and bottom halves is also observed in the 2D axisymmetric model. Therefore, the numerical errors in the 2D axisymmetric models are too high to be considered reliable.

5.2 Effect of interface resistance

The peak temperature reached in the simulation with no interface resistance is only $218\,^0$C, whereas the peak temperature is $1230\,^0$C when the interface resistance is incorporated. Clearly, simulations which do not incorporate sheet-sheet interface resistance will be very inaccurate. This also serves to show the importance of incorporating accurate temperature-dependent interface resistance.

5.3 Effect of welding current on temperature profile

As expected, the size of the molten pool and peak temperature increases with increase in welding current. The weld pool appears to be an ellipse when viewed from a cross section parallel to the axis of symmetry and passing through the center. The weld nugget diameter does not appear to increase substantially with increase in current. This may be due to the higher sheet-sheet interface resistance of galvanized sheets when compared to uncoated sheets.

5.4 Evolution of temperature profile with time

The temperature at the center, which lies on the sheet-sheet interface, is higher than all other points, as the major source of resistance (and hence heat) is at the sheet-sheet interface. The cooling rate is initially quite steep, and reduces as the temperatures reduce. The curves appear to be consistent with Newton's law of cooling. Interestingly, the temperature difference between the center and the point 0.2 mm below the center along the axis of symmetry appears to be nearly constant.

CHAPTER 6

Conclusions

- 2D axisymmetric model was found to give inaccurate results and hence must not be used for simulating resistance spot welding.
- Accurate temperature-dependent sheet-sheet interface resistance is necessary in order to obtain accurate temperature profiles in simulations.
- Weld nugget diameter was found to increase with increase in current.
- COMSOL Multiphysics was successfully used to simulate resistance spot welding.

REFERENCES

[1] Status of the vehicular pollution control programme in India, March 2010, Central Pollution Control Board, Ministry of Environment and Forests, Govt. of India.

[2] Hon'ble Supreme Court of India in the matter "Air Pollution of Delhi and NCR" of M.C. Mehta vs. Union of India CWP-13029 of 1985.

[3] Central Pollution Control Board, Ministry of Environment and Forests, Govt. of India.

[4] Regulation (EU) No 333/2014 of the European Parliament and of the Council of 11 March 2014: "Amending Regulation (EC) No 443/2009 to define the modalities for reaching the 2020 target to reduce CO 2 emissions from new passenger cars", March 2014.

[5] T. Kondo, K Ishiuchi, "1.2 GPa Advanced High Strength Steel with High Formability", SAE Technical Paper, 2014-01-0991, 2013.

[6] D.K. Matlock and J.G. Speer, "Third Generation of AHSS: Microstructure Design Concepts in Microstructure and Texture in Steels", Springer, pp. 185-205, 2009.

[7] Murugaiyan Amirthalingam, E. M. van der Aa, C. Kwakernaak, M. J. M. Hermans and I. M. Richardson, "Elemental segregation during resistance spot welding of boron containing advanced high strength steels", Welding in the world pp. 743-755, 2015.

[8] P. Eftekharimilani, E. M. van der Aa, M. J. M. Hermans and I. M. Richardson, 'The microstructural evolution and elemental distribution of a 3rd generation 1 GPa advanced high strength steel during double pulse resistance spot welding", Welding in the world pp. 691-701, 2017.

[9] E. M. van der Aa, M. Amirthalingam, J. Winter, D. N. Hanlon, M. J. M. Hermans, M. Rijnders and I. M. Richardson, 'Improved resistance spot weldability of 3rd generation AHSS for automotive applications', Mathematical modelling of weld phenomena vol. 11, 2015.

[10] M. Pouranvari and S. P. H. Marashi, "Critical review of automotive steels spot welding: process, structure and properties", Science and Technology of Welding and Joining, Vol. 18, No. 5, pp. 361-403, 2013.

[11] R. Wu, A. J. Freeman and G. B. Olson, "First principles determination of the effects of phosphorus and boron on iron grain boundary cohesion', Science vol. 265, pp. 376–380, 1994.

[12] David Loveborn, "3D FE Simulations of Resistance Spot Welding", degree project in engineering mechanics, KTH, Stockholm, 2016.

[13] H. Zhang and J. Senkara, "Resistance Welding: Fundamentals and Applications", Boca Raton: CRC Press, 2006.

[14] O. Andersson, "Process planning of resistance spot welding," KTH, Stockholm, 2013.

[15] K. Zhou and L. Cai, "Study on effect of electrode force on resistance spot welding process", Journal of Applied Physics, vol. 116, no. 8, 2014.

[16] ISO 5182:2008 Resistance welding - Materials for electrodes and ancillary equipment.

[17] ISO 5821:2009 Resistance Welding - Spot welding electrode caps.

[18] J.A. Greenwood, ‘Temperature in Spot Welding”, British Welding Journal, vol. 9, pp. 316-322, 1961.

[19] Gould, J. E,, “An Examination of Nugget Development During Spot Welding, Using Both Experimental and Analytical Techniques", Welding Journal, Vol. 66, No. 1, pp. 1-10,1987.

[20] Cho, H. S., and Cho, Y. J., "A Study of Thermal Behaviour in Resistance Spot Welds," Welding Journal, Vol. 68, No. 6, pp. 236-244, 1989.

[21] Han, Z,, Orozco, J., Indacochea, J. E. and Chen, C. H., "Resistance Spot Welding: A Heat Transfer Study," Welding Journal, Vol. 68, No. 9, pp. 363-371, 1989.

[22] Wei, P. S,, and Ho, C. Y,, "Axisymmetric Nugget Growth During Resistance Spot Welding," ASME Journal of Heat Transfer, Vol. 112, No. 2, pp. 309-316, 1990.

[23] Wei, P. S., and Yeh, C. Y,, "Factors Affecting Nugget Growth With Mushy-Zone Phase Change During Resistance Spot Welding," ASME Journal of Heat Transfer, Vol. 113, No. 8, pp. 643-649, 1991.

[24] Nishiguchi, K,, and Matsuyama, K., "Influence of Current Wave Form on Nugget Formation Phenomena When Spot Welding Thin Steel Sheet," Welding in the World, Vol. 25, o. 11/12, pp. 222-244, 1987.

[25] H.Huh and W.J. Kang, “Electrothermal analysis of electric resistance spot welding by a 3-D finite element method” Journal of material technology, vol.63, pp.672-677, 1997.

[26] M.A. Ninshu and Murakawa, “Numerical and Experimental Study on Nugget Formation in Resistance Spot Welding for High Strength Steel Sheets in Automobile Bodies”, Transactions of Joining and Welding Research Institute (JWRI), Vol.38 No. 2, 2009.

[27] J.A Khan, L. Xu, and Y.J Chao, “Prediction of nugget development during resistance spot welding using coupled thermal-electrical-mechanical model”, Science and technology of welding and joining, Vol.04 No: 04, 1999.

[28] Zhigang Houa, Soo Kimb, Yuanxun Wang, Chunzhi Li and Chuanyao Chena, “Finite element analysis for the mechanical features of resistance spot welding process”, Journal of Materials Processing Technology 185, pp.160–165, 2007.

[29] Guo Zhong, “Finite element analysis of resistance spot welding process”, Chinese Control and Decision Conference, CCDC 2009.

[30] M.Hamedi and H Pashazadeh, “Numerical study of the nugget formation in resistance spot welding”, International Journal of Mechanics, Issue 1 Volume 2 ,2008.

[31] Hamid Eisazadeh, Mohsen Hamedi and Ayob Halvaee, “New parametric study of nugget size in resistance spot welding process using finite element method”, Materials and Design vol. 31, pp.149–157, 2010.

[32] Thakur.A.G, Rasane.A.R and Nandedkar.V.M, “Finite element analysis of resistance spot welding nugget formation”, International Journal of Applied Engineering and Research, Dindigul, Volume 1, No: 3, 2010.

[33] B. Le Gloannec, O. Doyen, C. Pouvreau, A. Doghri and A. Poulon-Quintin, "Numerical simulation of resistance upset welding in rod to tube configuration with contact resistance determination", Journal of Materials Processing Technology 238, pp.409–422, 2016.

[34] Feulvarch, E., Rogeon, P., Carré, P., Robin, V., Sibilia, G. and Bergheau J.M., "Resistance spot welding process: experimental and numerical modeling of the weld growth mechanisms with consideration of contact conditions", Numerical heat transfer Part A: Applied, 49, pp.345–367, 2006.

[35] Robin, V., Sanchez, A., Soigneux, J. and Bergheau, J.M., "Numerical simulation of spot welding with special attention to contact conditions", Mathematical Modelling of Weld Phenomena 6. Maney, Graz, Austria, pp. 997–1013, 2002.

[36] S.S. Babu, M.L. Santella, Z. Feng, B.W. Riemer and J.W. Cohron, "Empirical model of effects of pressure and temperature on electrical contact resistance of metals", Science and Technology of Welding and Joining, 6:3, pp.126-132, 2001.

[37] Quanfeng Song, Wenqi Zhang and Niels Bay, "An Experimental Study Determines the Electrical Contact Resistance in Resistance Welding", Welding research, May, pp.73-76, 2005.

[38] Ye-feng Bao, Ling Ren, Zhong-tai Yu, Yong-feng Jiang and Ke Yang, "An experimental study on contact resistance of coated galvanized steel sheet", Welding in the World 62, pp. 511-516, 2018.

[39] N. Saunders, U. K. Z. Guo, X. Li, A. P. Miodownik and J. -Ph. Schillé, "Using JMatPro to model materials properties and behaviour", Journal of Materials, pp. 55-60, 2003.

[40] Amitava De and O P Gupta, "An Improved Numerical Modeling for Resistance Spot Welding Process and Its Experimental Verification", Journal of Manufacturing Science and Engineering, Vol. 120, pp. 246-251, 1998.

[41] J. A. Greenwood, "Constriction resistance and the real area of contact", British Journal of Applied Physics, vol. 17, 1966.

[42] M. G. Cooper, B. B. Mikic, and M. M. Yovanovich, "Thermal contact conductance," International Journal of Heat and Mass Transfer, vol. 12, no. 3, pp. 279–300, 1969.